# Optimized Compact-support Interpolation Kernels

Ramtin Madani, *Student Member, IEEE,* Ali Ayremlou, *Student Member, IEEE,* Arash Amini, Farrokh Marvasti, *Senior Member, IEEE,*

***Abstract*—In this paper, we investigate the problem of designing compact-support interpolation kernels for a given class of signals. By using calculus of variations, we simplify the optimization problem from an nonlinear infinite dimensional problem to a linear finite dimensional case, and then find the optimum compact-support function that best approximates a given filter in the least square sense ($\ell_2$ norm). The benefit of compact-support interpolants is the low computational complexity in the interpolation process while the optimum compact-support interpolant guarantees the highest achievable Signal to Noise Ratio (SNR). Our simulation results confirm the superior performance of the proposed kernel compared to other conventional compact-support interpolants such as cubic spline.**

***Index Terms*—Compact-Support, Filter Design, Interpolation, Spline.**

## I. Introduction

DUE the existence of powerful digital tools, nowadays it is very common to convert the continuous time signals into the discrete form, and after discrete processing, we can convert it back to the original domain. The conversion of the continuous signal into the discrete domain is usually called the sampling process; the common form of sampling consists of taking samples directly from the continuous signal at equidistant time instants (uniform sampling). Although the samples are uniquely determined by the continuous function, there are infinite number of continuous signals which produce the same set of samples. The reconstruction process is defined as selecting one of the infinite possibilities which satisfies certain constraints. For a given set of constraints, a proper sampling scheme is the one that establishes a one-to-one mapping between the discrete signals and the set of continuous functions satisfying the constraints. One of the well-known constraints is the finite support in Fourier domain [**?**]. The theory of wavelets [**?**], [**?**], [**?**] introduced a generalized class of basis for representing continuous functions. In fact, any kind of such representation is equivalent to associating a countable infinite set of scalars (coefficients) to any given continuous function (similar to sampling). The one-to-one mapping of this association is achieved only if the continuous function belongs to a specific class. The reconstruction of the continuous function from the coefficients usually involves filter banks and interpolation. Multiresolution analysis [**?**], [**?**], self-similarity [**?**], [**?**], and singularity analysis [**?**] are inseparable from continuous-time interpolation. Theoretically, the optimum interpolations require interpolants with infinite support which are impractical from the implementation perspective. The common trend is to truncate the interpolant function or approximate it with a compact-support function.

In this field, polynomial splines such as B-Splines are particularly popular, mainly due to their simplicity, compact-support, and excellent approximation capabilities compared to other methods. B-Spline interpolations have spread to various applications [**?**], [**?**], [**?**]. The cubic spline is of particular interest since it generates the function with minimum curvature passing through a given set of points [**?**]. Also fast methods for obtaining the spline coefficients of a continuous function is addressed in [**?**]; it is shown that the coefficients follow a recursive equation. For the asymptotic behaviour (as order increases) and approximation properties of the B-splines, the interested reader is referred to [**?**].

Many advantages of the B-splines arise from the fact that they are compact-support functions. However, there is no evidence that they are the best compact-support kernels for the interpolation process; i.e., it may be possible to improve the performance without compromising the desired property of the compact-supportedness. In this paper, we focus on the problem of designing compact-support interpolants that best resemble a given filter such as the ideal lowpass filter; more precisely, we aim to find a compact-support kernel that minimizes the least squared error when its cardinal is compared to a given function. The given filter may be any arbitrary function that reflects the properties and constraints of the class of signals that enter the sampling process. Different variations of this problem are previously studied in [**?**], [**?**]: the problem in [**?**] is to find the best one-sided (causal) kernel (not necessarily with compact-support) while in [**?**], the aim is to convert the required IIR filtering in the discrete domain for a given polynomial spline to an optimal causal filtering. The optimal B-spline interpolants for hexagonal 2D signals are also derived in [**?**]. The main difference of the work in this paper from the aforementioned problems is that we do not restrict the kernel to be a polynomial spline. In fact, the optimality of the kernel is within the linear combination of the Dirichlet functions (see Def. 7 for the definition of Dirichlet functions); i.e., one cannot improve the least squared error by modifying the resultant compact-support kernel with an additive Dirichlet function.

The remainder of the paper is organized as follows: The next section briefly describes the spline interpolation method. In section III, a novel scheme is proposed to produce new optimized kernels for interpolation regardless of the type of filtering. The performance of the proposed method is evaluated in section IV by comparing the interpolation results of the proposed method to those of well-known interpolation techniques. Section V concludes the paper.

All authors are with Advanced Communications Research Institute (ACRI), the Department of Electrical Engineering, Sharif University of Technology, Tehran, Iran, e-mails: {r_madani , a_ayremlou , arashsil}@ee.sharif.edu, marvasti@sharif.ir

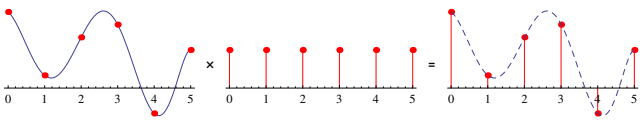

Fig. 1. Sampling process modelled by multiplying an impulse train by a continuous time signal.

## II. Preliminaries

We start by introducing some of the definitions required in the rest of the paper. The definitions and results are generic to the dimension of the space, therefore, instead of the 1D terms "continuous-time" and "discrete-time", we use "continuous-space" and "discrete-space", respectively. Furthermore, $\mathbf{t}$ represents the index for the continuous-space signals while $\mathbf{n}$ plays the same role for the discrete-space signals. To facilitate the reading of the paper, we have gathered all the notations in Table I.

*Definition* 1. For a continuous-space $k$-dimensional signal $x(\mathbf{t})$, the continuous-space signal $x_p(\mathbf{t})$ and the discrete-space signal $x_d(\mathbf{n})$ are defined as follows:

$$x_d[n_1, n_2, \ldots, n_k] \triangleq x(n_1 T, n_2 T, \ldots, n_k T), \tag{1}$$

$$x_p(\mathbf{t}) \triangleq x(\mathbf{t})p(\mathbf{t}) = \sum_{\mathbf{n}\in\mathbb{Z}^k} x_d[\mathbf{n}]\delta(\mathbf{t} - T\mathbf{n}), \tag{2}$$

where $\delta(\mathbf{t})$ is the $k$-dimensional Dirac delta distribution centred at origin and $p(\mathbf{t}) \triangleq \sum_{n\in\mathbb{Z}^k} \delta(\mathbf{t} - T\mathbf{n})$ is the $k$-dimensional periodic impulse train. The sampling period $T$ is normalized to 1 in all directions. without any loss of generality.

The sampling process is shown in Fig 1.

*Definition* 2. A Linear Shift Invariant (LSI) filter with impulse response $h(\mathbf{t})$ is said to have the "interpolation property" if and only if,

$$h_p(\mathbf{t}) = \delta(\mathbf{t}). \tag{3}$$

In other words, the interpolation property implies that the impulse response vanishes at the integers or in general at the grid points. This is equivalent to the *partition of unity* in the 1D case.

*Definition* 3. A discrete-space signal $y_d[\mathbf{n}]$ is called a "proper" signal if and only if it is bounded and has a unique and bounded inverse $y_d^{-1}[\mathbf{n}]$.

It is not hard to check that a bounded discrete signal is proper if and only if it contains no zeros (and obviously no poles) on the unit circle.

*Definition* 4. For any continuous-space signal $y(\mathbf{t})$, if $y_d[\mathbf{n}]$ is a proper signal, then $\widehat{y}(\mathbf{t})$ is defined as follows:

$$\widehat{y}(\mathbf{t}) = \left((y_p)^{-1} * y\right)(\mathbf{t}). \tag{4}$$

TABLE I
Notations and Definitions

| Notation | Definition |
|---|---|
| $\delta(\mathbf{t})$ | $k$-dimensional Dirac delta function |
| $p(\mathbf{t})$ | $k$-dimensional periodic impulse train |
| $x_d[\mathbf{n}]$ | $x(\mathbf{n}T)$ (See Def. 1) |
| $x_p(\mathbf{t})$ | $x(\mathbf{t})p(\mathbf{t})$ (See Def. 1) |
| $y_d^{-1}[\mathbf{n}]$ | Inverse of $y_d[\mathbf{n}]$ (i.e, $y_d[\mathbf{n}] * y_d^{-1}[\mathbf{n}] = \delta(\mathbf{t})$) |
| $\widehat{y}(\mathbf{t})$ | $\left((y_p)^{-1} * y\right)(\mathbf{t})$ (See Def. 4) |
| $\beta^m(t)$ | The polynomial B-Spline of degree $m$ (See Def. 5) |
| $c^m(t)$ | Cardinal spline of degree $m$ (See Def. 6) |
| $D^k$ | Set of all $k$-dimensional continuous-space signals that satisfy the Dirichlet conditions (See Def. 7) |
| $\chi^m(y_d)$ | Feasible set (See Def. 8) |
| $e_x(y)$ | Cost function (See Def. 9) |
| $\rho^m[x, \rho_d^m]$ | Optimized compact-support interpolation kernel (See Def.10) |
| $\mathcal{F}\{x\}$ | $k$-dimensional continuous-space Fourier transform operator |
| $\mathbf{M}_{x_d}^{a,b}$ | Convolution matrix (See Def. 11) |
| $\mathbf{v}_x^{a,b}$ | Convolution vector (See Def. 12) |

*Corollary* 1. $\widehat{y}(\mathbf{t})$ in (4) is the impulse response of a filter with the interpolation property. In other words:

$$\widehat{y}_p(\mathbf{t}) = \delta(\mathbf{t}). \tag{5}$$

*Proof:*

$$\begin{aligned} \widehat{y}_p(\mathbf{t}) &= \widehat{y}(\mathbf{t})p(\mathbf{t}) \\ &= \left[\left((y_p)^{-1} * y\right)(\mathbf{t})\right] p(\mathbf{t}) \\ &= \left((y_p)^{-1} * y_p\right)(\mathbf{t}) = \delta(\mathbf{t}). \end{aligned} \tag{6}$$

■

*Definition* 5. The polynomial B-Spline of degree $m$ is defined as:

$$\beta^m(t) \triangleq \sum_{n=0}^{m+1} (-1)^n \binom{m+1}{n} u^{m+1}(t-n). \tag{7}$$

*Definition* 6. According to the above definition, $c^m(t) \triangleq \widehat{\beta^m}(t)$ defines as the cardinal spline of degree $m$ (Fig. 2).

## III. Proposed Optimized Compact-support Kernels

In many applications, it is desirable that the interpolation filter resembles an ideal filter, and there is no need for it either to be smooth or piecewise polynomial. In this section an optimized compact-support interpolation kernel will be introduced to emulate a desired filter.

*Definition* 7. Let $D^k$ denote the set of all $k$-dimensional continuous-space signals that satisfy the Dirichlet conditions, i.e, for any $y(\mathbf{t}) \in D^k$:

1) $y(\mathbf{t})$ has a finite number of extrema in any given box,
2) $y(\mathbf{t})$ has a finite number of discontinuities in any given box,

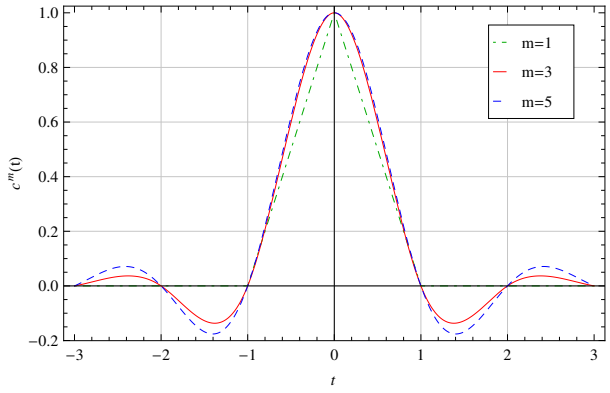


Fig. 2. Cardinal splines of different degrees.

3) $y(\mathbf{t})$ is absolutely integrable over a period,
4) $y(\mathbf{t})$ is bounded.

To continue, we first introduce an affine subspace of the $k$-dimensional Dirichlet function space (functions that satisfy Dirichlet conditions) and then, we find the optimal interpolation kernel within this subspace by means of the calculus of variation.

*Definition* 8. Let $y_d[\mathbf{n}]$ be a proper signal that vanishes at all $\mathbf{n} \notin (0, m+1)^k$. For this particular $y_d$, define $\chi^m(y_d)$ as the set of all continuous-space signals $y(\mathbf{t})$ that satisfy,

1) $y \in D^k$,
2) $\forall \mathbf{n} \in \mathbb{N}^k; \quad y(\mathbf{n}) = y_d[\mathbf{n}]$,
3) $\forall \mathbf{t} \notin (0, m+1)^k; \quad y(\mathbf{t}) = 0$.

In plain words, $\chi^m(y_d)$ is a set of continuous-space compact support functions for which the set of samples coincides with $y_d[\mathbf{n}]$. The use of $y(\mathbf{t}) \in \chi^m(y_d)$ as an interpolation kernel for interpolating $x_d[\mathbf{n}]$ establishes a linear shift invariant process with the impulse response $\widehat{y}(\mathbf{t})$.

*Definition* 9. The error function $e_x \colon \chi^m(y_d) \to \mathbb{R}$ is defined as follows:

$$\begin{aligned} e_x(y) &\triangleq \| \widehat{y} * x_p - x \|_2^2 \\ &= \int_{\mathbb{R}^k} |(\widehat{y} * x_p)(\mathbf{t}) - x(\mathbf{t})|^2 d\mathbf{t} \\ &= \int_{\mathbb{R}^k} |\mathcal{F}\{\widehat{y} * x_p\} - \mathcal{F}\{x\}|^2 d\mathbf{f} \\ &= \int_{\mathbb{R}^k} |\mathcal{F}\{\big((y_p)^{-1} * y\big) * x_p\} - \mathcal{F}\{x\}|^2 d\mathbf{f} \\ &= \int_{\mathbb{R}^k} |\frac{\mathcal{F}\{x_p\}}{\mathcal{F}\{y_p\}} \mathcal{F}\{y\} - \mathcal{F}\{x\}|^2 d\mathbf{f}. \end{aligned} \tag{8}$$

where $\mathcal{F}$ represents the $k$-dimensional continuous-space Fourier transform operator.

*Definition* 10. According to the above definition, if $\rho_d^m$ is a proper signal that vanishes at all $\mathbf{n} \notin (0, m+1)^k$, an optimal compact-support kernel $\rho^m[x, \rho_d^m]$ is defined by:

$$\rho^m[x, \rho_d^m] \triangleq \underset{y \in \chi^m(\rho_d^m)}{\arg\min}\, e_x(y). \tag{9}$$

Now, for a given proper discrete signal $\rho_d^m$ with the required vanishing property, we employ the calculus of variations in order to find the optimized continuous interpolation kernel $\rho^m$ that minimizes the error function $e_x(\rho^m)$.

*Theorem* 1. Equation (9) has a unique solution and it satisfies

$$[x_p * \overline{x_p} * (\rho_p^m)^{-1} * (\overline{\rho_p^m})^{-1}] * \rho^m = [(\overline{\rho_p^m})^{-1} * \overline{x_p}] * x, \tag{10}$$

for all $\mathbf{t} \in (0, m+1)^k$, where $\overline{y}(\mathbf{t}) \triangleq y^*(-\mathbf{t})$.

*Proof:* For $\gamma \in \chi^m(0)$ and any $\varepsilon > 0$, we have $\rho^m + \varepsilon\gamma \in \chi^m(\rho_d^m)$, and the variational derivative of $e_x(\rho^m)$ with respect to $\rho^m$ with $\gamma$ as the test function is equal to

$$\begin{aligned} \langle e_x(\rho^m), \gamma \rangle &\triangleq \lim_{\varepsilon \to 0} \frac{e_x(\rho^m + \varepsilon\gamma) - e_x(\rho^m)}{\varepsilon} \\ &= 2 \int_{\mathbb{R}^k} \Re\{\gamma(\mathbf{t})\} \Re\Bigg\{ \mathcal{F}^{-1}\Bigg\{ \left[\frac{\mathcal{F}\{x_p\}}{\mathcal{F}\{\rho_p^m\}}\right]^* \\ &\quad \left[\frac{\mathcal{F}\{\rho^m\}}{\mathcal{F}\{\rho_p^m\}} \mathcal{F}\{x_p\} - \mathcal{F}\{x\}\right] \Bigg\}\Bigg\} d\mathbf{t} \\ &- 2 \int_{\mathbb{R}^k} \Im\{\gamma(\mathbf{t})\} \Im\Bigg\{ \mathcal{F}^{-1}\Bigg\{ \left[\frac{\mathcal{F}\{x_p\}}{\mathcal{F}\{\rho_p^m\}}\right]^* \\ &\quad \left[\frac{\mathcal{F}\{\rho^m\}}{\mathcal{F}\{\rho_p^m\}} \mathcal{F}\{x_p\} - \mathcal{F}\{x\}\right] \Bigg\}\Bigg\} d\mathbf{t} \end{aligned} \tag{11}$$

The proof of (11) is presented in (12). Since there are no boundaries for $\chi^m(\rho_d^m)$, the minimizers of $e_x(\rho^m)$ are those that set $\langle e(\rho^m), \gamma \rangle$ to zero for all $\gamma \in \chi^m(0)$. This implies that the second term inside the above integral should be zero for $\mathbf{t} \in (0, m+1)^k$, i.e,

$$\mathcal{F}^{-1}\Bigg\{ \left[\frac{\mathcal{F}\{x_p\}}{\mathcal{F}\{\rho_p^m\}}\right]^* \left[\frac{\mathcal{F}\{\rho^m\}}{\mathcal{F}\{\rho_p^m\}} \mathcal{F}\{x_p\} - \mathcal{F}\{x\}\right] \Bigg\} = 0. \tag{13}$$

The above equation directly yields (10). Since we have a quadratic minimization problem subject to an affine feasible set $\chi^m(\rho_d^m)$, the problem is convex and has a unique solution. ■

### A. Filter Estimation

**Another** application of (10) is to approximate an ideal interpolation filter by an optimized compact-support kernel. In fact, these kernels are superior to **FIR filters**.

Now the goal is to design $\rho^m$ such that $\widehat{\rho^m}$ best estimations $h$, the impulse response of a filter that has the interpolation property.

*Lemma* 1. (Estimating a desired filter) Assume $h(\mathbf{t})$ is the impulse response of a linear shift invariant filter which satisfies the interpolation property and let $\rho_d^m[\mathbf{n}]$ be a proper discrete signal, then

$$\underset{y \in \chi^m(\rho_d^m)}{\arg\min}\, \|h - \widehat{y}\|_2^2 = \rho^m[h, \rho_d^m]. \tag{14}$$

$$
\begin{aligned}
\langle e_x(\rho^m[x,\rho_d^m]),\gamma\rangle &\triangleq \lim_{\varepsilon\to 0}\frac{e_x(\rho^m+\varepsilon\gamma)-e_x(\rho^m)}{\varepsilon}\\
&= \lim_{\varepsilon\to 0}\frac{1}{\varepsilon}\left[\int_{\mathbb{R}^k}\left|\left(\frac{\mathcal{F}\{\rho^m+\varepsilon\gamma\}}{\mathcal{F}\{(\rho^m+\varepsilon\gamma)p\}}\right)\mathcal{F}\{x_p\}-\mathcal{F}\{x\}\right|^2 d\mathbf{f}-\int_{\mathbb{R}^k}\left|\left(\frac{\mathcal{F}\{\rho^m\}}{\mathcal{F}\{\rho_p^m\}}\right)\mathcal{F}\{x_p\}-\mathcal{F}\{x\}\right|^2 d\mathbf{f}\right]\\
&= \lim_{\varepsilon\to 0}\frac{1}{\varepsilon}\int_{\mathbb{R}^k}\left\{\left[\Re\left\{\left(\frac{\mathcal{F}\{\rho^m+\varepsilon\gamma\}}{\mathcal{F}\{(\rho^m+\varepsilon\gamma)p\}}\right)\mathcal{F}\{x_p\}-\mathcal{F}\{x\}\right\}^2-\Re\left\{\left(\frac{\mathcal{F}\{\rho^m\}}{\mathcal{F}\{\rho_p^m\}}\right)\mathcal{F}\{x_p\}-\mathcal{F}\{x\}\right\}^2\right]\right.\\
&\quad\left.+\left[\Im\left\{\left(\frac{\mathcal{F}\{\rho^m+\varepsilon\gamma\}}{\mathcal{F}\{(\rho^m+\varepsilon\gamma)p\}}\right)\mathcal{F}\{x_p\}-\mathcal{F}\{x\}\right\}^2-\Im\left\{\left(\frac{\mathcal{F}\{\rho^m\}}{\mathcal{F}\{\rho_p^m\}}\right)\mathcal{F}\{x_p\}-\mathcal{F}\{x\}\right\}^2\right]\right\}d\mathbf{f}\\
&= \lim_{\varepsilon\to 0}\frac{1}{\varepsilon}\int_{\mathbb{R}^k}\left\{\Re\left\{\left(\frac{\mathcal{F}\{\rho^m+\varepsilon\gamma\}}{\mathcal{F}\{(\rho^m+\varepsilon\gamma)p\}}-\frac{\mathcal{F}\{\rho^m\}}{\mathcal{F}\{\rho_p^m\}}\right)\mathcal{F}\{x_p\}\right\}\Re\left\{\left(\frac{\mathcal{F}\{\rho^m+\varepsilon\gamma\}}{\mathcal{F}\{(\rho^m+\varepsilon\gamma)p\}}+\frac{\mathcal{F}\{\rho^m\}}{\mathcal{F}\{\rho_p^m\}}\right)\mathcal{F}\{x_p\}-2\mathcal{F}\{x\}\right\}\right.\\
&\quad\left.+\Im\left\{\left(\frac{\mathcal{F}\{\rho^m+\varepsilon\gamma\}}{\mathcal{F}\{(\rho^m+\varepsilon\gamma)p\}}-\frac{\mathcal{F}\{\rho^m\}}{\mathcal{F}\{\rho_p^m\}}\right)\mathcal{F}\{x_p\}\right\}\Im\left\{\left(\frac{\mathcal{F}\{\rho^m+\varepsilon\gamma\}}{\mathcal{F}\{(\rho^m+\varepsilon\gamma)p\}}+\frac{\mathcal{F}\{\rho^m\}}{\mathcal{F}\{\rho_p^m\}}\right)\mathcal{F}\{x_p\}-2\mathcal{F}\{x\}\right\}\right\}d\mathbf{f}\\
&= \lim_{\varepsilon\to 0}\frac{1}{\varepsilon}\int_{\mathbb{R}^k}\left\{\Re\left\{\left(\frac{\mathcal{F}\{\rho^m+\varepsilon\gamma\}-\mathcal{F}\{\rho^m\}}{\mathcal{F}\{\rho_p^m\}}\right)\mathcal{F}\{x_p\}\right\}\Re\left\{\left(\frac{\mathcal{F}\{\rho^m+\varepsilon\gamma\}+\mathcal{F}\{\rho^m\}}{\mathcal{F}\{\rho_p^m\}}\right)\mathcal{F}\{x_p\}-2\mathcal{F}\{x\}\right\}\right.\\
&\quad\left.+\Im\left\{\left(\frac{\mathcal{F}\{\rho^m+\varepsilon\gamma\}-\mathcal{F}\{\rho^m\}}{\mathcal{F}\{\rho_p^m\}}\right)\mathcal{F}\{x_p\}\right\}\Im\left\{\left(\frac{\mathcal{F}\{\rho^m+\varepsilon\gamma\}+\mathcal{F}\{\rho^m\}}{\mathcal{F}\{\rho_p^m\}}\right)\mathcal{F}\{x_p\}-2\mathcal{F}\{x\}\right\}\right\}d\mathbf{f}\\
&= \lim_{\varepsilon\to 0}\frac{1}{\varepsilon}\int_{\mathbb{R}^k}\left\{\Re\left\{\left(\frac{\mathcal{F}\{\varepsilon\gamma\}}{\mathcal{F}\{\rho_p^m\}}\right)\mathcal{F}\{x_p\}\right\}\Re\left\{\left(\frac{\mathcal{F}\{2\rho^m+\varepsilon\gamma\}}{\mathcal{F}\{\rho_p^m\}}\right)\mathcal{F}\{x_p\}-2\mathcal{F}\{x\}\right\}\right.\\
&\quad\left.+\Im\left\{\left(\frac{\mathcal{F}\{\varepsilon\gamma\}}{\mathcal{F}\{\rho_p^m\}}\right)\mathcal{F}\{x_p\}\right\}\Im\left\{\left(\frac{\mathcal{F}\{2\rho^m+\varepsilon\gamma\}}{\mathcal{F}\{\rho_p^m\}}\right)\mathcal{F}\{x_p\}-2\mathcal{F}\{x\}\right\}\right\}d\mathbf{f}\\
&= \int_{\mathbb{R}^k}\Re\left\{\frac{\mathcal{F}\{\gamma\}}{\mathcal{F}\{\rho_p^m\}}\mathcal{F}\{x_p\}\right\}\Re\left\{2\frac{\mathcal{F}\{\rho^m\}}{\mathcal{F}\{\rho_p^m\}}\mathcal{F}\{x_p\}-2\mathcal{F}\{x\}\right\}\\
&\quad+\Im\left\{\frac{\mathcal{F}\{\gamma\}}{\mathcal{F}\{\rho_p^m\}}\mathcal{F}\{x_p\}\right\}\Im\left\{2\frac{\mathcal{F}\{\rho^m\}}{\mathcal{F}\{\rho_p^m\}}\mathcal{F}\{x_p\}-2\mathcal{F}\{x\}\right\}d\mathbf{f}\\
&= 2\Re\left\{\int_{\mathbb{R}^k}\left[\frac{\mathcal{F}\{\gamma\}}{\mathcal{F}\{\rho_p^m\}}\mathcal{F}\{x_p\}\right]\left[\frac{\mathcal{F}\{\rho^m\}}{\mathcal{F}\{\rho_p^m\}}\mathcal{F}\{x_p\}-\mathcal{F}\{x\}\right]^* d\mathbf{f}\right\}\\
&= 2\Re\left\{\int_{\mathbb{R}^k}\mathcal{F}\{\gamma\}\left[\frac{\mathcal{F}\{x_p\}}{\mathcal{F}\{\rho_p^m\}}\right]\left[\frac{\mathcal{F}\{\rho^m\}}{\mathcal{F}\{\rho_p^m\}}\mathcal{F}\{x_p\}-\mathcal{F}\{x\}\right]^* d\mathbf{f}\right\}\\
&= 2\Re\left\{\int_{\mathbb{R}^k}\gamma(\mathbf{t})\mathcal{F}^{-1}\left\{\left[\frac{\mathcal{F}\{x_p\}}{\mathcal{F}\{\rho_p^m\}}\right]^*\left[\frac{\mathcal{F}\{x_p\}}{\mathcal{F}\{\rho_p^m\}}\mathcal{F}\{\rho^m\}-\mathcal{F}\{x\}\right]\right\}\right\}d\mathbf{t}\\
&= 2\int_{\mathbb{R}^k}\Re\{\gamma(\mathbf{t})\}\Re\left\{\mathcal{F}^{-1}\left\{\left[\frac{\mathcal{F}\{x_p\}}{\mathcal{F}\{\rho_p^m\}}\right]^*\left[\frac{\mathcal{F}\{x_p\}}{\mathcal{F}\{\rho_p^m\}}\mathcal{F}\{\rho^m\}-\mathcal{F}\{x\}\right]\right\}\right\}d\mathbf{t}\\
&\quad-2\int_{\mathbb{R}^k}\Im\{\gamma(\mathbf{t})\}\Im\left\{\mathcal{F}^{-1}\left\{\left[\frac{\mathcal{F}\{x_p\}}{\mathcal{F}\{\rho_p^m\}}\right]^*\left[\frac{\mathcal{F}\{x_p\}}{\mathcal{F}\{\rho_p^m\}}\mathcal{F}\{\rho^m\}-\mathcal{F}\{x\}\right]\right\}\right\}d\mathbf{t}
\end{aligned}
\tag{12}
$$

---

*Proof:*

$$
\begin{aligned}
e_h(y) &= \int_{-\infty}^{\infty}|\mathcal{F}\{\widehat{y}*h_p\}-\mathcal{F}\{h\}|^2 d\mathbf{f}\\
&= \int_{-\infty}^{\infty}|\mathcal{F}\{\widehat{y}\}\mathcal{F}\{h_p\}-\mathcal{F}\{h\}|^2 d\mathbf{f}\\
&= \int_{-\infty}^{\infty}|\mathcal{F}\{\widehat{y}\}-\mathcal{F}\{h\}|^2 d\mathbf{f}\\
&= \|h-\widehat{y}\|_2^2. \qquad (15)
\end{aligned}
$$

Thus

$$
\arg\min_{y\in\chi^m(\rho_d^m)}\|h-\widehat{y}\|_2^2 = \arg\min_{y\in\chi^m(\rho_d^m)} e_h(y) = \rho^m[h,\rho_d^m]. \qquad (16)
$$

■

*Corollary* 2. For an impulse response $h(\mathbf{t})$ with the interpolation property, if $\rho^m\in\chi^m(\rho_d^m)$ denotes the optimum compact-support kernel for which $\widehat{\rho^m}$ best approximates $h(\mathbf{t})$ (i.e., $\widehat{\rho^m}(\mathbf{t}) = \arg\min_{y\in\chi^m(\rho_d^m)}\|h-\widehat{y}\|_2^2$), then $\rho^m\in\chi^m(\rho_d^m)$ satisfies:

$$
[(\rho_p^m)^{-1}*(\overline{\rho_p^m})^{-1}]*\rho^m = [(\overline{\rho_p^m})^{-1}]*h. \qquad (17)
$$

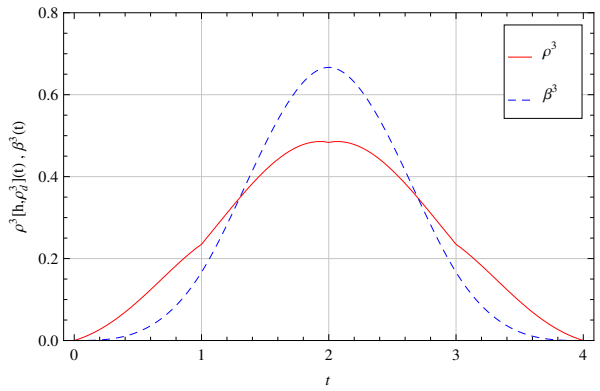


Fig. 3. The optimized compact-support interpolation kernel versus cubic B-spline. $\rho^3\{h,\rho_d^3\}$ is the optimized kernel built for estimating the ideal lowpass filter $h(t)=\frac{\sin(\pi t)}{\pi t}$ with $\rho_d^3(z)=0.235z+0.484z^2+0.235z^3$.

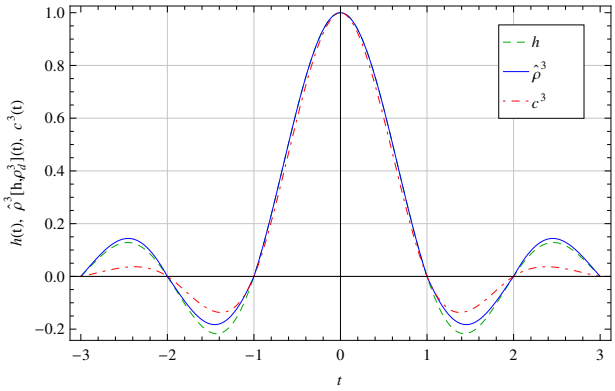


Fig. 4. The comparison of the proposed method with the cubic spline for an ideal lowpass filter.

The proof follows directly from (10) and the fact that $h(\mathbf{t})$ has the interpolation property.

Figure 3 shows the cubic B-spline and the optimized interpolation kernel designed for estimating the ideal lowpass filter $h(t)=sinc(t)$ with $\rho_d^3(z)=0.235z+0.484z^2+0.235z^3$, while Fig. 4 shows $\widehat{\rho^3}[h,\rho_d^3](t)$ in comparison to $c^3(t)$.

### B. Implmentational Details in 1D

It is proven that the optimized interpolation kernel which gives the best estimation of $x$ satisfies (10). By defining

$$v_p \triangleq (x_p * \overline{x_p}) * [(\rho_p^m)^{-1} * (\overline{\rho_p^m})^{-1}] \quad (18)$$

$$w \triangleq [(\overline{\rho_p^m})^{-1} * \overline{x_p}] * x, \quad (19)$$

for $k=1$, we can rewrite (10) as $(v_p * \rho^m)(t) = w(t)|_{t\in(0,m+1)}$. Since this equation is valid only in a particular interval, $(v_p)^{-1}$ cannot be used to obtain $\rho^m$. However, since $v_p$ is an impulse train (convolution of four impulse trains) we will show that the continuous functional equation in (10) boils down to solving a finite Hermitian Toeplitz system of linear equations. For this purpose, we first propose the notion of the convolution matrix and then, define two vectors containing functions which are supported only on a unit-length interval:

*Definition* 11. For a discrete-space one-dimensional signal $x_d[n]$, and any $a,b\in\mathbb{Z}$, the matrix $\mathbf{M}_{x_d}^{a,b} \triangleq [x_d[i-j+a]]_{i,j=1,\dots,b+1}$ is defined as the convolution matrix:

$$\mathbf{M}_{x_d}^{a,b} = \begin{bmatrix} x_d[a] & x_d[a-1] & \dots & x_d[a-b] \\ x_d[a+1] & x_d[a] & \dots & x_d[a-b+1] \\ \vdots & \vdots & \ddots & \vdots \\ x_d[a+b] & x_d[a+b-1] & \dots & x_d[a] \end{bmatrix}. \quad (20)$$

*Definition* 12. For a continuous-space one-dimensional signal $x(t)$, and any $a,b\in\mathbb{Z}$, the convolution vector is defined as $\mathbf{v}_x^{a,b}=[x_a,x_{a+1},\dots,x_{a+b}]^T$, where for $n\in\mathbb{Z}$ we have

$$x_n(t) = \begin{cases} x(t+n) & 0\le t<1 \\ 0 & \text{o.w.} \end{cases}. \quad (21)$$

Now, the matrix-form equivalent of the property (10) can be written as

$$\mathbf{M}_{v_d}^{0,m}\mathbf{v}_{\rho^m}^{0,m} = \mathbf{v}_w^{0,m}. \quad (22)$$

Since $v_d[-n]=v_d^*[n]$, the matrix $\mathbf{M}_{v_d}^{0,m}$ is both Hermitian and Toeplitz. An efficient recursive method for solving this kind of linear systems is presented in [**?**]. By solving (22), we can derive $\{\rho_n^m\}_{n=0}^m$ and thus, the optimized compact-support kernel:

$$\rho^m(t)=\sum_{n=0}^{m}\rho_n^m(t-n). \quad (23)$$

This optimized compact-support interpolation kernel minimizes the interpolation mean squared error. On the other hand, smoothness of the kernel and causality of the prefilter can be achieved by adjusting $\rho_d$.

### C. Implementational Details in 2D

In 2D case, to derive the optimized compact-support interpolation kernel $\rho^m(t_1,t_2)$ from (10), we have an $(m+1)^2$ by $(m+1)^2$ Toeplitz-block-Toeplitz linear system to solve:

$$\mathbf{M}_{(m+1)^2\times(m+1)^2}\mathbf{p}_{(m+1)^2\times1} = \mathbf{w}_{(m+1)^2\times1}, \quad (24)$$

where,

$$\mathbf{M} = \begin{bmatrix} \mathbf{M}_{v_d[0,.]}^{0,m} & \mathbf{M}_{v_d[-1,.]}^{0,m} & \dots & \mathbf{M}_{v_d[-m,.]}^{0,m} \\ \mathbf{M}_{v_d[1,.]}^{0,m} & \mathbf{M}_{v_d[0,.]}^{0,m} & \dots & \mathbf{M}_{v_d[-1,.]}^{0,m} \\ \vdots & \vdots & \ddots & \vdots \\ \mathbf{M}_{v_d[m,.]}^{0,m} & \mathbf{M}_{v_d[m-1,.]}^{0,m} & \dots & \mathbf{M}_{v_d[0,.]}^{0,m} \end{bmatrix}, \quad (25)$$

and

$$\mathbf{p} = \begin{bmatrix} \mathbf{v}_{\rho^m(0,.)}^{0,m} \\ \mathbf{v}_{\rho^m(1,.)}^{0,m} \\ \vdots \\ \mathbf{v}_{\rho^m(m,.)}^{0,m} \end{bmatrix}, \mathbf{w} = \begin{bmatrix} \mathbf{v}_{w(0,.)}^{0,m} \\ \mathbf{v}_{w(1,.)}^{0,m} \\ \vdots \\ \mathbf{v}_{w(m,.)}^{0,m} \end{bmatrix}. \quad (26)$$

According to [**?**], the linear system (24) can be solved by $O(m^5)$ steps and the solution can be obtained from the derived

vector as follows:

$$\rho^m(t_1,t_2)=\sum_{n_1=0}^{m}\sum_{n_2=0}^{m}P_{n_1(m+1)+(n_2+1)}(t_1-n_1,t_2-n_2). \tag{27}$$

## IV. Simulation Results

To compare the proposed method with the existing interpolation techniques, we have performed various simulations. The cubic B-spline, due to its short time support and relatively high accuracy in approximating the ideal lowpass filter, is the most common technique for interpolating 1-D lowpass signals. For the purpose of comparison, we have optimized a kernel with the same time support as an ideal lowpass filter. Figures 3 and 4 show the shape of the obtained kernel and the interpolating spline, respectively. Figure 3 shows that the energy is more concentrated in the middle of the cubic B-spline while the optimized kernel has slower decaying rate of energy at the sides. The resultant interpolation kernels, as depicted in Fig. 4, reveal that the main advantage of the optimized kernel ($\hat{\rho}^3$) compared to the cubic spline ($c^3$), is the smaller error in the first side-lobe. The SNR values of $\hat{\rho}^3$ and $c^3$ with respect to the $sinc$ function are $20.39$ and $13.15$dBs, respectively.

For a more realistic comparison, we have applied different interpolation techniques on standard test images. For this purpose, the original images, with or without applying the anti-aliasing filter (ideal lowpass filter), are down-sampled by a factor 2 in each direction ($25\%$ of the original pixels) and then they are enlarged (zooming) using the interpolation techniques. The comparison is made with the following interpolation methods: 1) bilinear interpolation, 2) bicubic interpolation, 3) wavelet-domain zero padding cycle-spinning [**?**], and 4) soft-decision estimation technique for adaptive image interpolation [**?**]. Also for our proposed method, two different scenarios are implemented: the ideal filter for which we are optimizing the kernel function is first taken as a $sinc$ filter, and first the spectrum of the original image.

In order to evaluate the quality of the interpolated images, we have considered the Peak Signal-to-Noise Ratio (PSNR) criterion. Table II indicates the resultant PSNR values when the original image is subject to the anti-aliasing filter before down-sampling while the error is calculated based on the image without applying the filter. Table III contains similar values while the basis for the error calculation is the anti-aliased image. In both cases, the PSNR criterion the proposed optimized kernel for the ideal lowpass ($sinc$) filter. On the average, the proposed method out performs the other standard interpolating methods by $0.74$dB in Table II and $4.19$dB in Table III.

To exclude the effect of the anti-aliasing filter, the simulations are repeated without applying it and the results are presented in Table IV. As expected, the optimized kernel which is matched to the spectrum of the original image outperforms other competitors in all cases. It should be mentioned that the function $\rho^m[x,\rho_d^m]$ is not a universal filter in this case and depends on the choice of the image.

Although the PSNR value is a good measure of global quality of an image, it does not reflect the local properties. In order to present a qualitative view of various interpolation methods, we have plotted the enlarged images for a segment of the Lena test image in Fig. 5. To highlight the differences, one could compare the texture on the top and the sharpness on the bottom edge of the hat.

## V. Conclusion

The interpolation problem using uniform knots is a well studied subject. In this paper, we considered the problem of optimizing the interpolation kernel for a given class of signals (represented by a filter). Although functional optimization in the continuous domain is often very difficult, we have demonstrated the equivalency of this problem with a finite dimensional linear problem which can be easily solved using linear algebra. As a special case, we considered the class of lowpass signals which is associated with the sinc function as the optimum interpolation kernel. For the optimum compact-support interpolant, we compared our function with the conventional cubic B-Spline; the simulation results indicate 1dB improvement in the SNR of the interpolated signal (on the average) using the introduced function, and 7dB improvement compared to the cardinal spline itself (compared to the sinc function) (Fig. 4).

## Acknowledgment

The authors would like to thank Prof. M. Unser from EPFL and Dr. R. Razvan from the mathematical sciences department of Sharif university for their helpful comments.

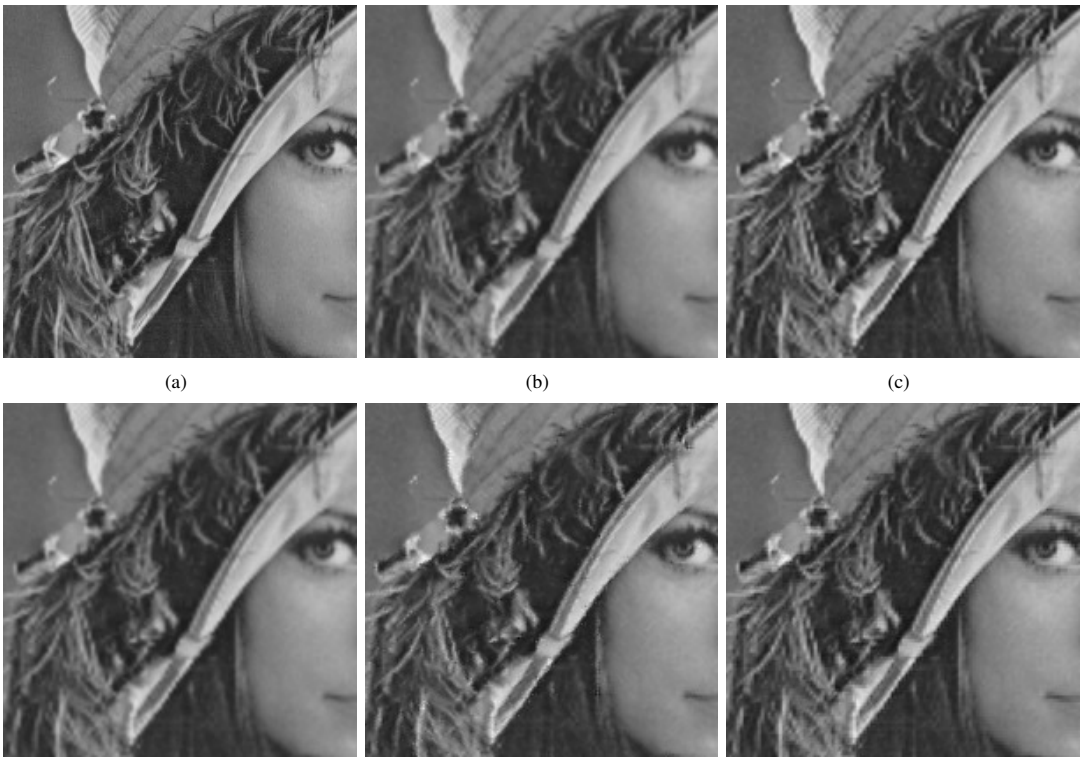

(a) (b) (c)

(d) (e) (f)

Fig. 5. Comparison of different methods for the Lena image: (a) The original image, (b) bilinear interpolation, (c) bicubic Interpolation. (d) WZP Cycle-Spinning [**?**], (e) SAI [**?**], and (f) the proposed method.

TABLE II
PSNR (dB) RESULTS OF THE RECONSTRUCTED IMAGES BY VARIOUS METHODS, THE ORIGINAL IMAGE WAS ANTI-ALIASED BEFORE SAMPLING AND THE RESULTS ARE COMPARED TO THE **ORIGINAL** IMAGE (IMAGE ENLARGEMENT FROM $256 \times 256$ TO $512 \times 512$)

| **Images** | Bilinear | Bicubic [**?**] | WZP–CS [**?**] | SAI [**?**] | Optimized kernel for image $\rho^3[x, \rho_d^3]$ | Optimized kernel for the ideal lowPass $\rho^3[sinc(t), \rho_d^3]$ |
|---|---|---|---|---|---|---|
| **Lena** | 30.33 | 30.44 | 30.12 | 30.96 | **32.46** | 32.20 |
| **Baboon** | 22.40 | 22.52 | 22.41 | 22.89 | 22.20 | **24.22** |
| **Barbara** | 24.39 | 24.42 | 24.34 | 24.65 | 24.33 | **25.14** |
| **Peppers** | 29.46 | 29.46 | 29.14 | 29.72 | **31.14** | 31.04 |
| **Girl** | 30.98 | 30.98 | 30.66 | 30.43 | **31.70** | 30.87 |
| **Fishing bout** | 27.68 | 27.48 | 28.12 | 30.92 | 28.61 | **29.71** |
| **Couple** | 27.35 | 27.50 | 27.27 | 27.39 | 28.04 | **28.97** |
| **Overall Average** | 27.51 | 27.54 | 27.43 | 28.14 | 28.35 | **28.88** |

TABLE III
PSNR (dB) RESULTS OF THE RECONSTRUCTED IMAGES BY VARIOUS METHODS, THE ORIGINAL IMAGE WAS ANTI-ALIASED BEFORE SAMPLING AND THE RESULTS ARE COMPARED TO THE **ANTI-ALIASED** IMAGE (IMAGE ENLARGEMENT FROM $256 \times 256$ TO $512 \times 512$)

| **Images** | Bilinear | Bicubic [**?**] | WZP–CS [**?**] | SAI [**?**] | Optimized kernel for image $\rho^3[x, \rho_d^3]$ | Optimized kernel for the ideal lowPass $\rho^3[sinc(t), \rho_d^3]$ |
|---|---|---|---|---|---|---|
| **Lena** | 31.56 | 31.72 | 31.62 | 32.45 | **35.28** | 35.21 |
| **Baboon** | 26.88 | 27.26 | 26.89 | 28.48 | 26.33 | **35.70** |
| **Barbara** | 30.61 | 30.74 | 30.65 | 31.86 | 30.40 | **35.72** |
| **Peppers** | 31.62 | 31.82 | 31.77 | 32.14 | 37.41 | **38.02** |
| **Girl** | 34.08 | 34.24 | 34.25 | 33.10 | **35.89** | 34.28 |
| **Fishing bout** | 29.91 | 30.19 | 29.93 | 30.92 | 32.00 | **34.87** |
| **Couple** | 29.81 | 30.10 | 29.84 | 29.77 | 31.44 | **34.28** |
| **Overall Average** | 30.64 | 30.87 | 30.71 | 31.25 | 32.68 | **35.44** |

TABLE IV
PSNR (DB) RESULTS OF THE RECONSTRUCTED IMAGES BY VARIOUS METHODS, THE **ORIGINAL IMAGE WAS NOT ANTI-ALIASED** AND THE RESULTS ARE COMPARED TO THE **ORIGINAL** IMAGE $256 \times 256$ TO $512 \times 512$)

| **Images** | Bilinear | Bicubic [**?**] | WZP–CS [**?**] | SAI [**?**] | Optimized kernel for image $\rho^3[x, \rho_d^3]$ | Optimized kernel for the ideal lowPass $\rho^3[sinc(t), \rho_d^3]$ |
|---|---|---|---|---|---|---|
| **Lena** | 30.21 | 30.13 | 30.05 | 30.88 | **32.29** | 30.95 |
| **Baboon** | 21.67 | 21.34 | 21.70 | 22.09 | **22.50** | 21.63 |
| **Barbara** | 23.90 | 23.32 | 23.88 | 23.71 | **25.10** | 22.58 |
| **Peppers** | 28.82 | 28.61 | 26.93 | 28.91 | **30.64** | 29.77 |
| **Girl** | 30.41 | 29.97 | 30.20 | 29.94 | **30.90** | 29.20 |
| **Fishing bout** | 27.10 | 26.93 | 27.07 | 27.63 | **28.50** | 27.66 |
| **Couple** | 26.92 | 26.73 | 26.86 | 26.93 | **27.91** | 27.08 |
| **Overall Average** | 27.00 | 26.72 | 26.67 | 27.16 | **29.12** | 26.98 |